UC Berkeley
UC Berkeley Previously Published Works

Title
Ultrahigh capacitive energy density in ion-bombarded relaxor ferroelectric films

Permalink
https://escholarship.org/uc/item/2zk6645k

Journal
Science, 369(6499)

ISSN
0036-8075

Authors
Kim, Jieun
Saremi, Sahar
Acharya, Megha
et al.

Publication Date
2020-07-03

DOI
10.1126/science.abb0631

Peer reviewed

DIELECTRICS

Ultrahigh capacitive energy density in ion-bombarded relaxor ferroelectric films

Jieun Kim[1], Sahar Saremi[1], Megha Acharya[1], Gabriel Velarde[1], Eric Parsonnet[2], Patrick Donahue[1], Alexander Qualls[2], David Garcia[1], Lane W. Martin[1,3]*

Dielectric capacitors can store and release electric energy at ultrafast rates and are extensively studied for applications in electronics and electric power systems. Among various candidates, thin films based on relaxor ferroelectrics, a special kind of ferroelectric with nanometer-sized domains, have attracted special attention because of their high energy densities and efficiencies. We show that high-energy ion bombardment improves the energy storage performance of relaxor ferroelectric thin films. Intrinsic point defects created by ion bombardment reduce leakage, delay low-field polarization saturation, enhance high-field polarizability, and improve breakdown strength. We demonstrate energy storage densities as high as ~133 joules per cubic centimeter with efficiencies exceeding 75%. Deterministic control of defects by means of postsynthesis processing methods such as ion bombardment can be used to overcome the trade-off between high polarizability and breakdown strength.

Dielectric materials can store charge and release it upon application and removal of an electric field. Electrostatic capacitors based on dielectrics have become key components in modern electronics and electric power systems because of their inherently fast charging and discharging rates and their high reliability (1–5). Capacitors generally have low energy densities relative to other energy storage systems such as batteries or fuel cells. The requirements for cost reduction and device miniaturization have driven rapid growth in research to develop dielectric capacitors that have high energy density, are efficient and reliable, and exhibit robust temperature stability (4).

One of the key parameters for energy storage in capacitors is the discharged-energy density U_d, defined as $\int_{P_{rem}}^{P_{max}} E dP$, where E is the electric field, P_{max} is the maximum polarization, and P_{rem} is the remanent polarization (6). The other key parameter is the efficiency $\eta = [U_d/(U_d + U_{loss})] \times 100(\%)$, where U_{loss} is the energy dissipated as a result of leakage or hysteresis and corresponds to the area inside the polarization–electric field hysteresis loop. To achieve high U_d and η, a dielectric capacitor should have a large change in polarization ($P_{max} - P_{rem}$) during discharge and a large breakdown electric field (E_b). These two characteristics are usually inversely correlated, $E_b = k^{-0.65}$ (where k is the dielectric constant), because of a sharper rise in local electric field in high-k materials (7). The focus of several investigations has been on optimizing the energy storage performance by inducing relaxor behavior to reduce P_{rem} in ferroelectrics with large

P_{max} and hysteresis (1), enhancing E_b in ferroelectrics with relaxor behavior (8), enhancing P_{max} of simple dielectrics with high E_b (9), or some combination thereof (2, 10).

Although the main idea for materials design has been to modify ferroelectrics into relaxors to exploit their delayed polarization saturation and relatively weak hysteresis through chemical doping or heterostructure design (1, 2, 4, 6, 11, 12), little is known about how to improve the energy storage performance of relaxors themselves. To achieve this, we propose a new strategy based on ion bombardment. By creating intrinsic point defects in epitaxial films of the prototypical relaxor ferroelectric 0.68Pb(Mg$_{1/3}$Nb$_{2/3}$)O$_3$-0.32PbTiO$_3$ (PMN-PT) using high-energy (3 MeV) helium ions that are made incident on PMN-PT postsynthesis (13), we can achieve simultaneous enhancement of switchable polarization ($P_{max} - P_{rem}$) and E_b. We demonstrate ultrahigh energy densities ($U_d > 130$ J/cm^3) with high efficiency ($\eta > 75\%$), excellent reliability ($>10^8$ cycles), and temperature stability ($-100°$ to $200°$C) in such ion-bombarded PMN-PT films.

Defects are, in general, thought to be deleterious to (relaxor) ferroelectrics and are blamed for high leakage currents, aging, and other negative effects (14). Recent studies have shown that defects produced by ion bombardment with high–kinetic energy species can be used to create favorable intrinsic point defects and complexes (e.g., defect dipoles), which can improve ferroelectric/electrical properties or even create novel function (15–25). Both point defects and defect dipoles or complexes can interact with free charge, producing deep-level trap states, or with polarization (biasing, pinning domain walls, etc.) (14). As a result, they have been used to induce numerous desirable effects such as enhancing electrical resistivity (15), tuning coercive fields and imprint and manipulating relaxor character (17), enhancing Curie temperatures (21), stabilizing morphotropic phase bound-

aries (22), driving large reversible piezoelectric strains (23), creating colossal permittivity (24), and even producing multistate stability (20, 25).

We illustrate the effect of ion bombardment on the PMN-PT films in a schematic of the ferroelectric polarization–electric field hysteresis loops for as-grown and ion-bombarded materials in Fig. 1A. Region 1 represents the presaturation regime where $E \ll E_b$ and $P < P_{sat}$ (saturation polarization) and is characterized by increased dielectric loss and P_{rem} with increasing E. Here, U_d and η are improved by lowering the effective dielectric constant k_{eff} (because the energy density during the charging cycle $U = \frac{1}{2}k_{eff}\varepsilon_0 E^2$, where ε_0 is the permittivity of free space) and lowering P_{rem}. Region 2 represents the postsaturation regime where $E \leq E_b$ and $P > P_{sat}$ and is characterized by nonlossy enhancement of polarization with increasing E. The lack of hysteresis is attributable either to polarization elongation after complete switching of the domains in ferroelectrics or to the fast dynamics of polarization fluctuations in relaxors (26). In this region, higher values of k_{eff} and E_b are advantageous to maximize the energy density. We observed highly nonlinear switching behavior, early polarization saturation, and moderate P_{rem} and E_b for as-grown PMN-PT films (Fig. 1A). The early polarization saturation and relatively low E_b result in small U_d (Fig. 1A, filled area). To improve the energy storage performance, we would like to delay polarization saturation and lower P_{rem} in region 1 and to induce high polarizability (k_{eff}) and high E_b in region 2.

We realized this by purposely increasing the concentration of intrinsic point defects (e.g., lead, titanium, and/or oxygen vacancies, etc.), which are created when helium ions knock target ions from their lattice sites (fig. S1). The increased defect concentration produces two beneficial effects: a reduction of leakage (15) and an introduction of stable imprint (i.e., a horizontal shift of the hysteresis loop) (17). The creation of charged point defects (e.g., V_{Pb}'', V_{Ti}''', $V_O^{\cdot\cdot}$, etc.) can, in turn, give rise to the formation of neutral defect dipoles (e.g., $V_O^{\cdot\cdot} - V_{Pb}''$, $V_O^{\cdot\cdot} - V_{Mg}''$, etc.) or more complicated defect complexes (e.g., $V_O^{\cdot\cdot} - V_{Ti}''' - V_O^{\cdot\cdot}$, etc.) to preserve charge neutrality (27, 28). Such defect dipoles can align their elastic and electric dipole moments along the elongated direction of the lattice and/or polarization directions (23). We controlled the defect-dipole alignment to be along the out-of-plane direction by growing PMN-PT films under small in-plane compressive strain, which leads to the appearance of an imprint in the hysteresis loops (17, 21, 29). At the same time, the formation of defect dipoles or complexes leads to a reduction of the leakage current by eliminating shallow-hole trap states such as isolated Pb^{3+} and V_{Pb}'' defects with small activation energies (~0.26 eV and ~0.56 eV, respectively) and forming deep-level trap states (~1 eV from the band edge) (30, 31).

[1]Department of Materials Science and Engineering, University of California, Berkeley, CA 94720, USA. [2]Department of Physics, University of California, Berkeley, CA 94720, USA. [3]Materials Sciences Division, Lawrence Berkeley National Laboratory, Berkeley, CA 94720, USA.
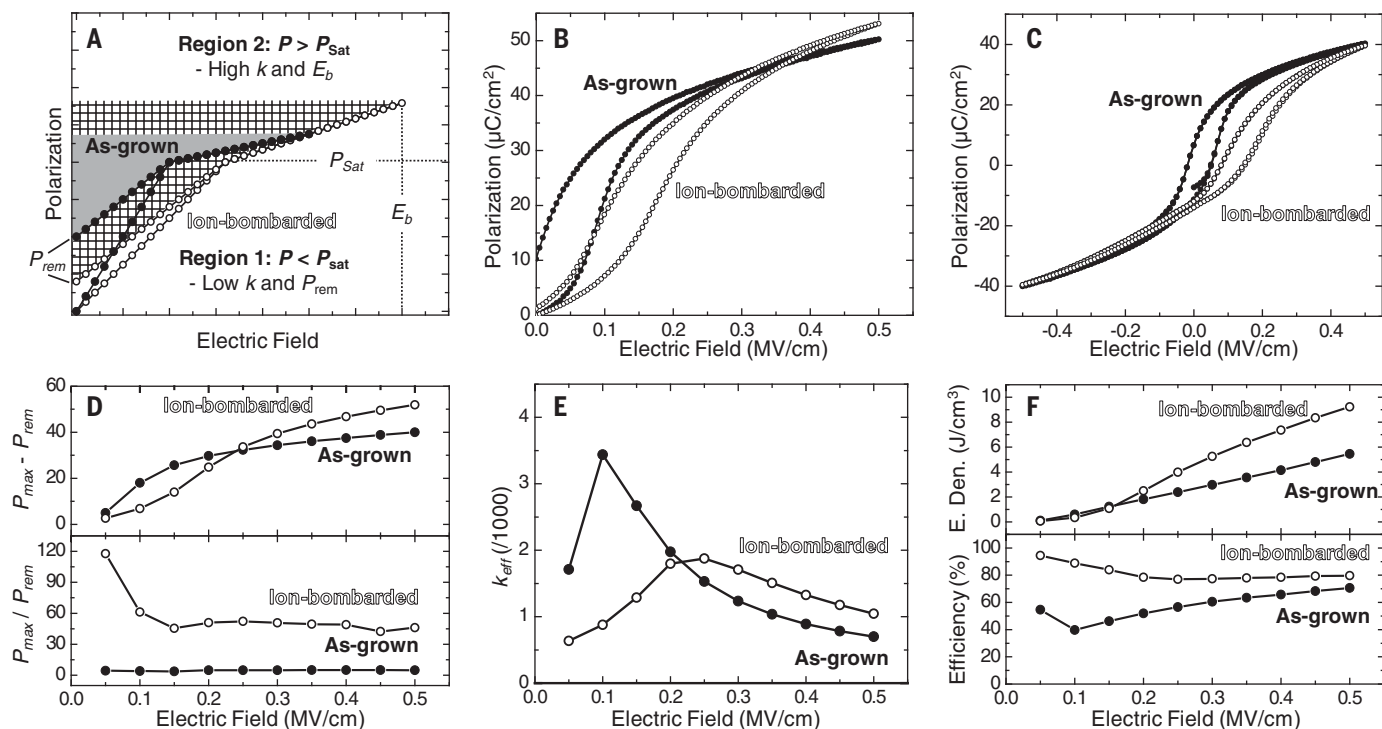*Corresponding author. Email: lwmartin@berkeley.edu

Fig. 1. Delayed polarization saturation and low-field energy storage properties. (**A**) Schematic illustrating the effect of ion bombardment on unipolar polarization–electric field hysteresis loops. Filled and cross-hatched areas in the hysteresis loops represent the energy density for as-grown and ion-bombarded films, respectively. Key features of the ion-bombarded state are indicated for each region. (**B** and **C**) Unipolar (B) and bipolar (C) hysteresis loops out to E = 0.5 MV/cm measured at 10 kHz. (**D** to **F**) $P_{max} - P_{rem}$ and P_{max}/P_{rem} (D), k_{eff} (E), and energy density (E. Den.) and efficiency (F) calculated from unipolar hysteresis loops.
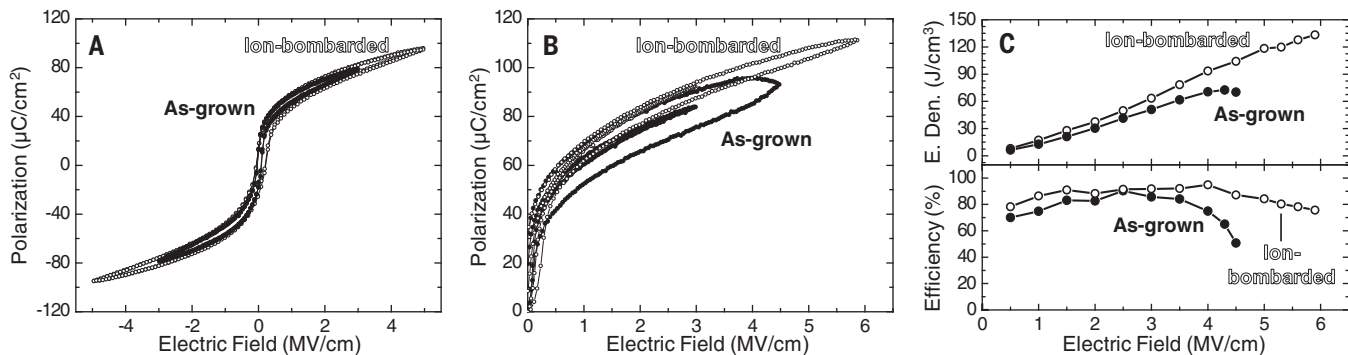
Fig. 2. High-field energy storage properties. (**A** and **B**) Bipolar (A) and unipolar (B) hysteresis loops at moderate and maximum E measured at 10 kHz. (**C**) Energy density and efficiency calculated from unipolar hysteresis loops.

In particular, we study 150-nm PMN-PT/ 25-nm $Ba_{0.5}Sr_{0.5}RuO_3/NdScO_3$ (110) heterostructures produced via pulsed-laser deposition. The samples are first patterned with 100-nm-thick $Ba_{0.5}Sr_{0.5}RuO_3$ circular top electrodes with a diameter of 25 μm (*13*). Smaller electrodes reduce the chance of extrinsic contributions to critical failure (e.g., pinholes) and are thus favorable for studying intrinsic properties (*13*). After device fabrication, half of the samples are uniformly exposed to ion bombardment (*13*). Although we have explored a range of ion doses, we focus on a dose of 3.33×10^{15} cm^{-2}, which provides the best combination of perform-

ance. Increasing the ion-bombardment dosage would further increase film resistance (*15*), but it also reduces relaxor character (*17*), which results in increased U_{loss} (i.e., reduced η) (fig. S2).

The PMN-PT heterostructures were highly crystalline, single-phase, stoichiometric, and coherently strained to the substrate (0.5% compressive strain) (figs. S3 to S6). We measured unipolar hysteresis loops by driving the top electrode in both the as-grown and ion-bombarded PMN-PT heterostructures with small magnitudes of positive electric field (Fig. 1B). The sign of the electric field was chosen to be the same as that of the imprint (*13*). Enhancement

of the low-field performance is important because real devices are typically operated at $E \ll E_b$ to avoid catastrophic failure. This requires avoiding materials design that pushes for larger U_d and η but results in poor low-field performance. Relative to the as-grown PMN-PT, ion-bombarded PMN-PT has lower P_{rem} and higher P_{max}. Examination of bipolar hysteresis loops (Fig. 1C) reveals that these differences arise from an increase in the magnitude of the self-polarization and imprint (the hysteresis loops for the as-grown and ion-bombarded PMN-PT are centered at 0.015 MV/cm and 0.115 MV/cm, respectively). This results in a
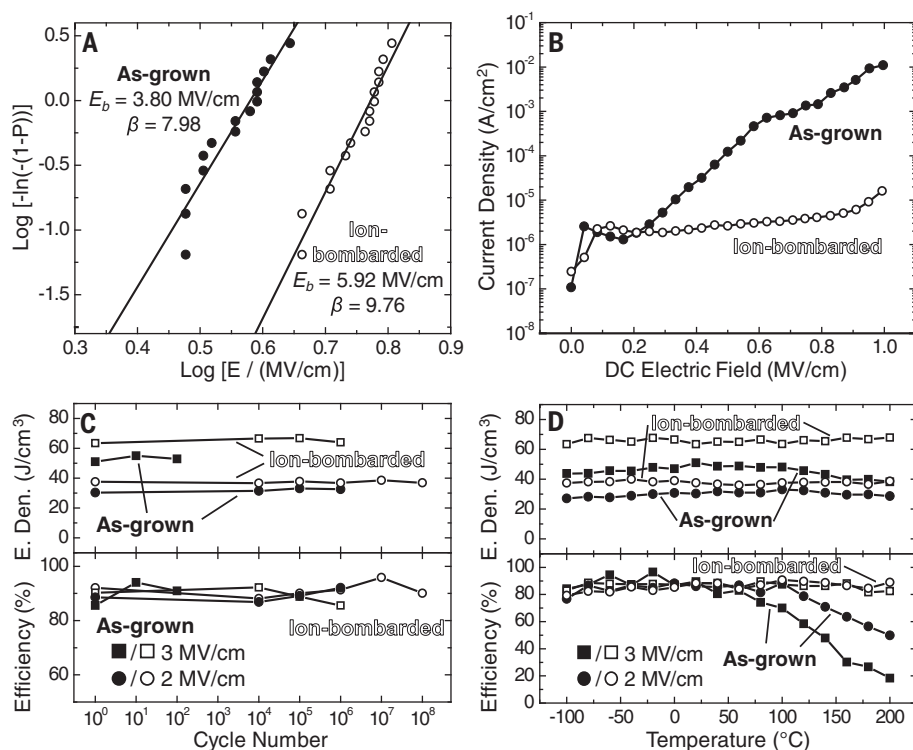
Fig. 3. Reliability and temperature stability. (**A**) Two-parameter Weibull distribution analysis of breakdown strengths. (**B**) Leakage current density as a function of dc electric field. (**C** and **D**) Fatigue test (C) and temperature dependence (−100° to 200°C) (D) of energy density and efficiency as a function of cycle number and temperature at E = 2 or 3 MV/cm and measured at 10 kHz.

larger magnitude of negative self-polarization (−13.2 μC/cm^2) in the ion-bombarded PMN-PT relative to the as-grown state (−7 μC/cm^2), which leads to larger P_{max} in the unipolar hysteresis loop (Fig. 1B) despite similar P_{max} under positive and negative fields (~40 μC/cm^2; Fig. 1C). The magnitude of $P_{max}^+ - P_{max}^-$ (~80 μC/cm^2) is in good agreement with previously reported values for PMN-PT thin films of similar composition (*32*). Plots of $P_{max} - P_{rem}$ and P_{max}/P_{rem} (Fig. 1D), k_{eff} (Fig. 1E), U_d, and η (Fig. 1F) calculated from the unipolar hysteresis loops (Fig. 1B) as a function of E reveal delayed polarization saturation below $E ≈ 0.25$ MV/cm at P_{sat} (~40 μC/cm^2) for the ion-bombarded PMN-PT. This behavior is consistent with suppressed extrinsic contributions to k (fig. S7). At $E > 0.25$ MV/cm, however, ion-bombarded PMN-PT shows higher k_{eff} (Fig. 1E), which is consistent with reduced tunability in ion-bombarded heterostructures (fig. S8). The combination of delayed polarization saturation, high k_{eff} after polarization saturation, and large P_{max}/P_{rem} resulted in higher U_d and η in ion-bombarded PMN-PT (Fig. 1F). These trends suggest enhanced energy storage performance at higher magnitudes of E.

We proceeded to examine the high-field energy storage performance by measuring bipolar hysteresis loops at maximum E before breakdown (Fig. 2A). The ion-bombarded PMN-PT withstands substantially larger E prior to breakdown. We measured unipolar hysteresis loops at various magnitudes of maximum E (Fig. 2B). The magnitudes of maximum E that we could apply to as-grown and ion-bombarded PMN-PT were ~4.5 MV/cm and ~5.9 MV/cm, respectively. At the maximum E, ion-bombarded PMN-PT maintains high η, as can be seen from the difference in U_{loss} (68 J/cm^3 at 4.5 MV/cm and 42.9 J/cm^3 at 5.9 MV/cm for the as-grown and ion-bombarded PMN-PT, respectively; Fig. 2B). We extracted U_d and η from the unipolar hysteresis loops (Fig. 2C). The maximum U_d for the ion-bombarded PMN-PT was 133.3 J/cm^3 (with a corresponding η of 75%) at 5.9 MV/cm. The U_d of ion-bombarded PMN-PT was enhanced by 84% relative to the as-grown PMN-PT while maintaining high η. Given that as-grown PMN-PT already exhibits U_d comparable to the highest reported value for lead-based systems (*33*), this combination of properties for the ion-bombarded films highlights the importance of postsynthesis processing to enhance energy storage performance.

Reliability and thermal stability are also key factors for discharge capacitors. As was seen in other performance metrics, the ion-bombarded PMN-PT also exhibited superior cyclability and temperature stability due to the enhanced breakdown strength. We obtained statistical values of E_b from testing 15 capacitors to fail- ure, and fitted the distribution of breakdown strengths to a standard Weibull distribution (Fig. 3A). We found the characteristic E_b (and Weibull modulus β, which represents the dispersion in the data) to be 3.80 ± 0.43 MV/cm (β = 7.98) and 5.92 ± 0.55 MV/cm (β = 9.76) for as-grown and ion-bombarded PMN-PT, respectively. Leakage current was also measured under dc electric field, and at E = 1 MV/cm it was found to be reduced by about three orders of magnitude in the ion-bombarded heterostructures (Fig. 3B). We attribute the reduction of leakage current in ion-bombarded PMN-PT to a delay of the onset of the bulk-limited Poole-Frenkel mechanism (fig. S9) (*13, 15*). We also probed the fatigue behavior by completing unipolar hysteresis loops after applying a 10-kHz triangular waveform at E = 1, 2, and 3 MV/cm for 10^x (x = 1, 2, 3, …, 8) cycles (Fig. 3C). At E = 1 MV/cm, both the as-grown and ion-bombarded PMN-PT maintained stable performance after >10^9 cycles (fig. S10). At E = 2 MV/cm, the as-grown PMN-PT broke down after 10^6 cycles, whereas the ion-bombarded PMN-PT remained stable even after 10^8 cycles. At E = 3 MV/cm, the as-grown PMN-PT broke down after 10^2 cycles and the ion-bombarded PMN-PT remained stable after 10^6 cycles.

We studied temperature stability by measuring unipolar hysteresis loops at E = 1, 2, and 3 MV/cm at a temperature range from −100° to 200°C (Fig. 3D). Similar to the fatigue behavior, both as-grown and ion-bombarded PMN-PT maintained stable performance at E = 1 MV/cm across the whole temperature range (fig. S10). At E = 3 MV/cm, the ion-bombarded PMN-PT showed excellent temperature stability of energy density (~63 J/cm^3) and efficiency (~80%) across the entire temperature range. In contrast, the as-grown PMN-PT showed lower energy density (~45 J/cm^3) and poorer efficiency (<60%) above 100°C, rendering it unsuitable for high-temperature operation. Typically, the enhancement of E_b comes at the cost of reduced energy density at the same magnitude of E, which requires a higher magnitude of E to be applied and thus limits the merit of higher E_b (*33*). This is not the case for ion-bombarded materials because of the simultaneous enhancement of low-field performance (Figs. 1F and 2C) and E_b (Fig. 3A), which leads to superior high-temperature performance in ion-bombarded PMN-PT relative to as-grown PMN-PT (U_d = 67.9 J/cm^3 and η = 82.5% versus U_d = 38.2 J/cm^3 and η = 18.4% at 3 MV/cm and 200°C).

Because ion bombardment can produce a variety of robust energy storage properties (i.e., energy density, efficiency, leakage current, fatigue resistance, and temperature stability) from intrinsic point defects, it holds promise as a way to improve energy storage performance. Future studies of the creation and control of defects by other processing routes (e.g., thermal treatment)

(*23, 28*) as well as optimization of growth processes with postsynthesis processing are highly desired. Ultimately, this approach could be applied to boost the energy performance of other relaxor-based energy storage capacitors.

REFERENCES AND NOTES

1. B. Chu *et al.*, *Science* **313**, 334–336 (2006).
2. H. Pan *et al.*, *Science* **365**, 578–582 (2019).
3. H. Palneedi, M. Peddigari, G.-T. Hwang, D.-Y. Jeong, J. Ryu, *Adv. Funct. Mater.* **28**, 1803665 (2018).
4. Q. Li *et al.*, *Nature* **523**, 576–579 (2015).
5. V. K. Prateek, V. K. Thakur, R. K. Gupta, *Chem. Rev.* **116**, 4260–4317 (2016).
6. B. Xu, J. Íñiguez, L. Bellaiche, *Nat. Commun.* **8**, 15682 (2017).
7. J. W. McPherson, J. Kim, A. Shanware, H. Mogul, J. Rodriguez, *IEEE Trans. Electron Dev.* **50**, 1771–1778 (2003).
8. Z. Sun *et al.*, *Adv. Mater.* **29**, 1604427 (2017).
9. L. Zhang *et al.*, *RSC Adv.* **7**, 8388–8393 (2017).
10. M. McMillen *et al.*, *Appl. Phys. Lett.* **101**, 242909 (2012).
11. L. Yang, X. Kong, Z. Cheng, S. Zhang, *J. Mater. Chem. A* **7**, 8573–8580 (2019).
12. Z. Yao *et al.*, *Adv. Mater.* **29**, 1601727 (2017).
13. See supplementary materials.
14. D. Damjanovic, *Rep. Prog. Phys.* **61**, 1267–1324 (1998).
15. S. Saremi *et al.*, *Adv. Mater.* **28**, 10750–10756 (2016).
16. B. Mei *et al.*, *APL Mater.* **7**, 111101 (2019).
17. S. Saremi, J. Kim, A. Ghosh, D. Meyers, L. W. Martin, *Phys. Rev. Lett.* **123**, 207602 (2019).
18. S. Saremi *et al.*, *Adv. Mater. Interfaces* **5**, 1700991 (2018).
19. S. Saremi, R. Gao, A. Dasgupta, L. W. Martin, *Am. Ceram. Soc. Bull.* **97**, 16–23 (2018).
20. S. Saremi *et al.*, *Phys. Rev. Mater.* **2**, 084414 (2018).
21. A. R. Damodaran, E. Breckenfeld, Z. Chen, S. Lee, L. W. Martin, *Adv. Mater.* **26**, 6341–6347 (2014).
22. A. Herklotz *et al.*, *Nano Lett.* **19**, 1033–1038 (2019).
23. X. Ren, *Nat. Mater.* **3**, 91–94 (2004).
24. W. Hu *et al.*, *Nat. Mater.* **12**, 821–826 (2013).
25. D. Lee *et al.*, *Adv. Mater.* **24**, 6490–6495 (2012).
26. D. Viehland, S. J. Jang, L. E. Cross, M. Wuttig, *J. Appl. Phys.* **68**, 2916–2921 (1990).
27. Y. Chiang, D. P. Birnie, W. D. Kingery, *Physical Ceramics* (Wiley, 1997).
28. J. F. Scott, C. A. Araujo, B. M. Melnick, L. D. McMillan, R. Zuleeg, *J. Appl. Phys.* **70**, 382–388 (1991).
29. W. L. Warren *et al.*, *J. Appl. Phys.* **79**, 9250–9257 (1996).
30. J. Robertson, W. L. Warren, B. A. Tuttle, D. Dimos, D. M. Smyth, *Appl. Phys. Lett.* **63**, 1519–1521 (1993).
31. Z. Zhang, P. Wu, L. Lu, C. Shu, *Appl. Phys. Lett.* **88**, 142902 (2006).
32. S. H. Baek *et al.*, *Science* **334**, 958–961 (2011).
33. X. Hao, Y. Wang, L. Zhang, L. Zhang, S. An, *Appl. Phys. Lett.* **102**, 163903 (2013).

Science

Ultrahigh capacitive energy density in ion-bombarded relaxor ferroelectric films

Jieun Kim, Sahar Saremi, Megha Acharya, Gabriel Velarde, Eric Parsonnet, Patrick Donahue, Alexander Qualls, David Garcia and Lane W. Martin

Defect-enhanced energy storage

Dielectric capacitors are vital components of electronics and power systems. The thin-film materials of which capacitors are composed are usually optimized by changing the material composition. However, Kim *et al.* found that postprocessing an already effective thin-film dielectric by high-energy ion bombardment further improved the material because of the introduction of specific types of defects that ultimately improved the energy storage performance. The results suggest that postprocessing may be important for developing the next generation of capacitors.

Science, this issue p. 81

ARTICLE TOOLS	http://science.sciencemag.org/content/369/6499/81
SUPPLEMENTARY MATERIALS	http://science.sciencemag.org/content/suppl/2020/07/01/369.6499.81.DC1
REFERENCES	This article cites 35 articles, 3 of which you can access for free http://science.sciencemag.org/content/369/6499/81#BIBL
PERMISSIONS	http://www.sciencemag.org/help/reprints-and-permissions

Use of this article is subject to the Terms of Service